JMEPEG (2011) 20:1505–1511
DOI: 10.1007/s11665-010-9824-9

1059-9495/$19.00

Slab Analysis of Ring Rolling Assuming Constant Shear Friction

A. Parvizi, K. Abrinia, and M. Salimi

(Submitted October 3, 2009; in revised form October 30, 2010)

In this article, an analytic solution for ring rolling process based on the slab method theory is presented, in which the non-uniformity of the normal and shear stresses across the section of the deforming material throughout the plastic region is considered. The friction factor multiplied by the shear yield strength ($\tau = mk$) is used to present friction between the main roll and the ring. The influence of the process parameters such as friction factor, feed speed, main roll rotational speed, and radii of the main roll and mandrel on process outputs is investigated. Complete expressions for the ring rolling pressure, force, and torque are obtained, and the position of neutral point is predicted. Comparison of the analytic results of this model with the experimental results of other investigators and FEM analysis show that they are in good agreement.

Keywords analytic solution, pressure distribution, ring rolling, slab method

1. Introduction

Ring rolling process is widely used to produce annular seamless rings from different materials in a wide range of dimensions. It is most often used to form steel rings, but has also been used for aluminum alloys, titanium alloys, composite metal rings, and polymers. These rings are manufactured from a bulk pierced billet through a complex sequence of radial or axial-radial rolling operations carried out in hot and cold working conditions (Ref 1). Large rings like those used in power generation plants, aircraft engines, or large cylindrical vessels are usually manufactured by hot ring rolling and small ones such as inner and outer bearing races by cold ring rolling.

The advantages of ring rolling include short production time, efficient use of material, uniform quality, smooth surfaces, and close geometrical tolerances which lead to considerable cost savings in terms of energy and labor. The main challenges in ring rolling technology are categorized into three branches: achievement of dimensional accuracy, surface quality, and a flawless product; achievement of different profiles from simple pre-forms, any material, ''right first time'' die design; and achievement of low total cost, low scrap, fast cycle times, low labor and energy input; little post-processing (Ref 2).

Over the years, some analytic, physical, and numerical modeling methods including experimental formulae (Ref 3), volume mapping (Ref 4), slip line fields method (Ref 5, 6), upper bound method (Ref 7, 8), and FE analysis (Ref 9, 10) are used by many researchers to predict the final results of ring rolling processes. The experimental formulae are generally limited to each class of ring rolling operations with specific

A. Parvizi and **K. Abrinia**, School of Mechanical Engineering, College of Engineering, University of Tehran, P. O. Box 11365-4563, Tehran, Iran; and **M. Salimi**, Department of Mechanical Engineering, Isfahan University of Technology, P. O. Box 84154, Isfahan, Iran. Contact e-mails: aliparvizi@ut.ac.ir and ali.parvizi@yahoo.com.

List of symbols

h	Variable ring thickness at the roll gap, m
h_1, h_2	Upper and lower element heights with respect to horizontal axis, respectively, m
h_i, h_o	Ring thicknesses at entry and exit of the roll gap, respectively, m
Δh	Decrease in ring thickness
k	Mean yield shear stress of the ring, pa
m	Friction factor of the main roll
n	Rotational speed of main roll, rad/s
r	Reduction in thickness, %
v	Feed speed (linear speed of mandrel), m/s
w	Width of the ring, m
x	Horizontal distance from the exit point in the roll gap, m
x_n	Neutral point of main roll, m
y	Vertical distance from the centerline of the ring, m
F_1, F_2	Main roll and mandrel rolling forces per unit width, respectively, N/m
L	The contact length, m
P_1, P_2	Main roll and mandrel rolling pressures, respectively, pa
$P_{1,II}$, $P_{1,II}$	Main roll pressures at the zones I and II, respectively, pa
R_1, R_2	Radii of main roll and mandrel, respectively, m
R_3	Inner radius of ring, m
R_{eq}	Equivalent work roll radius
R_m	Mean radius of ring, m
T	Rolling torque of the ring rolling process, N m
σ_1, σ_2	Normal stresses on vertical side of element at the top and bottom of the slab, respectively, pa
τ	Shear stress on vertical side of element, pa

materials and processing parameters; therefore, results cannot be generalized for other ring rolling operations. The volume mapping is capable of predicting the diametric growth in closed pass ring rolling operations but cannot predict roll forces or torques. The upper bound involves finding a kinematically admissible velocity field, which leads to a minimum forming energy. However, it is difficult to express an admissible velocity field for problems involving complex shapes and general material flow especially in transient conditions (Ref 11).

As the ring rolling process is non-steady state throughout and a large number of ring rotations are required to finish the product, it is different from the conventional rolling process. Therefore, the number of increments requires in numerical simulation of the process normally is several times that required for a regular metal-forming application. Although the FEM may be used to simulate this process accurately, it, however, involves excessive computation time and convergence problems due to the highly nonlinear nature of the process and the existence of complicated contact conditions (Ref 12).

The slab method can predict rapidly the rolling force and torque, and a large amount of CPU time can be saved. Therefore, this method is suitable for the ring rolling industry. Although numerous studies have used the slab method to investigate metal-forming processes like symmetric and asymmetric rolling characteristics (Ref 12-17), but this method has never been applied to ring rolling process. The major reason may have been the non-steady state characteristic throughout this process. In the previous studies on flat rolling (Ref 12), the slab method has been mainly applied with uniform distribution in shear stress. In the authors' previous study (Ref 13), this approach has been modified to non-uniform and linear distribution of stress while the constant shear friction was assumed. This approach has been adopted for the present study, applying the slab method to ring rolling process for the first time.

In this article, a solution based on the slab method of analysis is presented for ring rolling process. At first, a mathematical model for the stress field acting on a vertical slab in the roll gap is assumed in which the non-uniformity of the normal and shear stresses across the section of the deforming material is considered. Next, imposing the force balance on the slab with a differential thickness, one-dimensional differential equation for pressure at the roll gap is obtained. Finally, imposing relevant boundary conditions on the differential equation provides an analytic solution for the rolling pressure. In the analytic solution, a variety of factors for ring rolling process such as friction factor, feed speed (mandrel speed), main roll rotational speed, and radii of the main roll and mandrel have been used to investigate the behavior of the process. Based on this analysis, complete expressions for the ring rolling pressure, force, and torque are obtained, and the position of neutral point is determined.

2. Mathematical Models

The ring cross section at roll gap is rectangular with uniform unit thickness and heights, h_i and h_o, at entry and exit, respectively. The horizontal distance from the exit point in the roll gap is taken as the x-axis, and the origin is its intersection with the normal plane passing by the main roll and mandrel centers (Fig. 1).

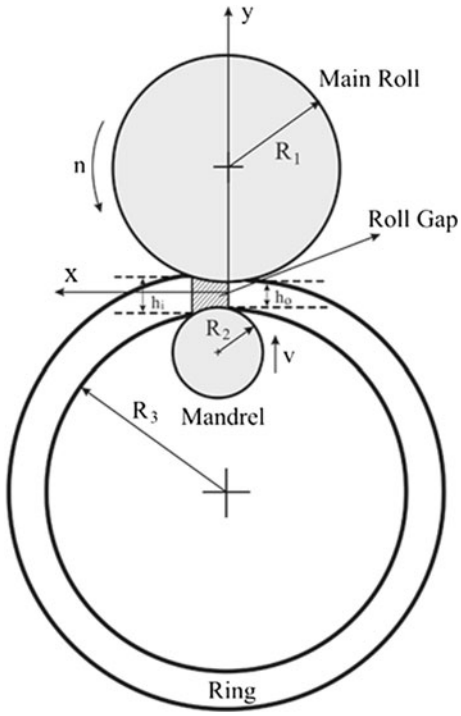

Fig. 1 Schematic illustration of ring rolling process

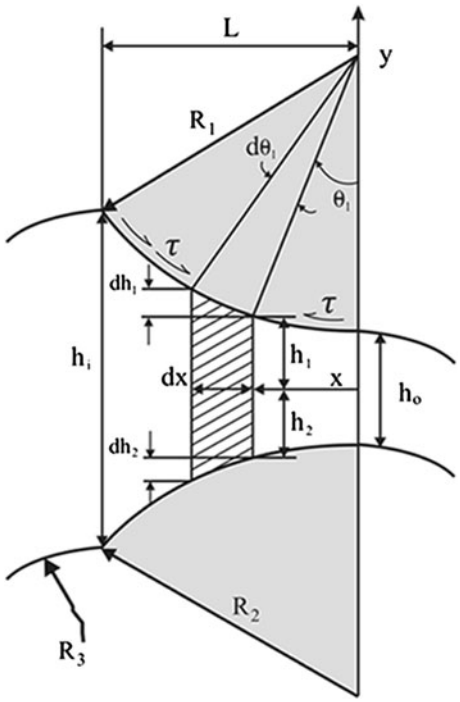

Fig. 2 Ring rolling geometry

The deforming region is defined as shown in Fig. 2 bounded by two flat surfaces, at the entry and exit and the surfaces of the main roll and the mandrel.

In the development of the mathematical model, it was assumed that the rolls are rigid and the material being rolled is rigid perfectly plastic. The plastic deformation occurs under plane strain conditions, so that material spread in transverse direction is ignored. The friction factor multiplied by the shear

yield strength ($\tau = mk$) is used to represent the interface friction between the main roll and the ring. The friction factor between the main roll and the ring is assumed to be constant along the contact length. As mandrel is free to rotate, it cannot afford any frictional moments. For simplicity, the friction at the interface between the mandrel and ring is neglected. The contact length is small as compared with the roll circumference and can be obtained from the following relationship (Ref 18):

$$L = \left[R_1^2 - \left\{ \frac{(R_1 + R_2 + h_o - h_i)^2 + R_1^2 - R_2^2}{2(R_1 + R_2 + h_o - h_i)} \right\}^2 \right]^{\frac{1}{2}} \quad \text{(Eq 1)}$$

where R_1 and R_2 are the radii of main roll and mandrel, respectively. Identifying the ring rolling loading effects is the first step in the development of equation of equilibrium for a differential vertical element in the roll gap. In passing through the roll gap (Fig. 2), the ring thickness is steadily reduced, and the ring radius and velocity progressively increased from entry to exit. The main roll surface speed is equal to an intermediate value between the ring entry and exit speeds. The point at which the ring and the main roll surface peripheral speeds are equal is called a neutral point. The ring is advanced by the frictional force acting toward the neutral point at entry and opposed by the frictional force acting at the exit region. Thus, the plastic deformation zone can be divided into two distinct regions: zone I from the exit to the neutral point; and zone II from the neutral point to the entry.

Subscripts 1 and 2 are designated to refer to quantities at the main roll and mandrel, respectively. From simple geometry,

$$h_1 = h_0/2 + x^2/2R_1 \quad h_2 = h_0/2 + x^2/2R_2 \quad \text{(Eq 2)}$$

where h_1 and h_2 are the upper and lower element heights with respect to horizontal axis, respectively. Hence in general

$$h = h_1 + h_2 = h_0 + x^2/R_{\text{eq}}, \quad R_{\text{eq}} = 2R_1R_2/(R_1 + R_2) \quad \text{(Eq 3)}$$

where h is variable ring thickness at the roll gap, and R_{eq} is equivalent work roll radius. If the slip between the main roll and the ring workpiece is neglected, then the circumference of the outer surface of the ring workpiece in one rotation is equal to the perimeter of the driven roll. Considering this fact, the decrease in ring thickness in any rotation is given by (Ref 19)

$$\Delta h = h_i - h_o = \frac{v}{n} \cdot \frac{(R_3 + h_o)}{R_1} \quad \text{(Eq 4)}$$

where v and n are the feed and rotational speeds of main roll, respectively, and R_3 is inner radius of ring. The equivalent stress field chosen for this purpose is shown in Fig. 3. This figure includes the non-uniformities of the stresses in the through thickness direction. The shear stresses on the vertical sides of the differential elements increase from zero at the bottom to the maximum values at the top which are equal to the ring-main roll interface friction. The normal and shear stresses on the vertical sides of the slab are assumed to be linearly distributed.

2.1 Ring Rolling Pressure

From the horizontal and vertical force equilibria based on the stress field of Fig. 3 and noting Fig. 1 and 2, the following relationships are obtained:

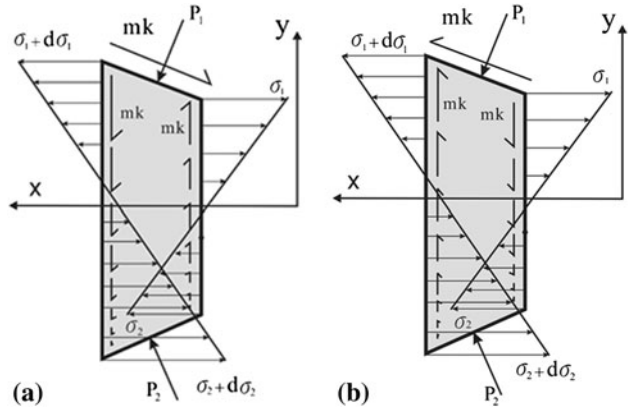

Fig. 3 Stress field acting on a vertical element at (a) entry zone II, and (b) exit zone I

$$(\sigma_1 - \sigma_2)\frac{dh}{2} + (d\sigma_1 - d\sigma_2)\frac{h}{2} + \left[P_1\left(\frac{x}{R_1}\right) + P_2\left(\frac{x}{R_2}\right) \pm mk \right] dx = 0 \quad \text{(Eq 5)}$$

$$-P_1 + P_2 \pm mk\left(\frac{1}{R_1} + \frac{1}{R_{\text{eq}}}\right)x = 0 \quad \text{(Eq 6)}$$

where σ_1 and σ_2 are normal stresses on the vertical side of element at the top and bottom of the slab respectively, P_1 and P_2 are the main roll and mandrel rolling pressures, respectively, m is the friction factor of the main roll, and k is the mean yield shear stress of the ring. The plus and minus signs in Eq 5 and 6 are designated to the zones I and II, respectively. The plane strain condition at any point in the plastic region gives

$$\tau_{xz} = \tau_{yz} = 0, \quad \varepsilon_z = 0 \quad \text{(Eq 7)}$$

where τ_{xz} and τ_{yz} are the shear stresses on the vertical side of the element, and ε_z is the normal strain in the z direction. Imposing the plane strain condition on the flow rule $(\varepsilon_z = 1/E(\sigma_z - 1/2(\sigma_x + \sigma_y)))$, results in

$$\sigma_z = (\sigma_x + \sigma_y)/2 \quad \text{(Eq 8)}$$

Using Eq 7 and 8 gives a two-dimensional Von-Mises yield criterion as follows [13]:

$$\left|(\sigma_x - \sigma_y)/2\right| = \sqrt{k^2 - \tau_{xy}^2} \quad \text{(Eq 9)}$$

Considering the method of the authors' previous study [16] and assuming small contact angle of the ring and the rolls, there are three different loading conditions for elements in the vertical slabs of Fig. 2. There are two elements on the top of any vertical slab and an element at the bottom. These elements are shown in Fig. 4.

Using the loading conditions of Fig. 3 for Eq 9, the yield criteria for the top and bottom elements on the vertical slabs take the following form:

$$\sigma_1 = -P_1 + 2k\sqrt{1 - m^2} \quad \sigma_2 = P_2 - 2k \quad \text{(Eq 10)}$$

Substituting Eq 10 and 6 into 5 and solving the subsequent one-dimensional differential equation, the main roll pressure distribution in zones I and II can be expressed as

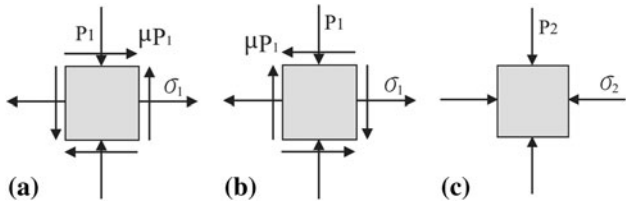

Fig. 4 Elements on the (a) top of the vertical slab at entry zone II, (b) top of the vertical slab at exit zone I, and (c) bottom of the vertical slab

$$P_1(x) = A_1 x + A_2 Ln\left(\frac{x^2}{R_{eq}} + h_o\right) + A_3 \arctan\left(\frac{x}{\sqrt{h_o R_{eq}}}\right) + C_1 \quad \text{(Eq 11)}$$

where C_1 is a constant which will be derived later and

$$A_1 = \pm mk\left(\frac{1}{R_1} + \frac{1}{R_{eq}}\right)\left(\frac{3}{2} - \frac{R_{eq}}{R_2}\right)$$
$$A_2 = k\left(1 + \sqrt{1 - m^2}\right)$$
$$A_3 = \pm mk\left[\left(\frac{1}{R_1} + \frac{1}{R_{eq}}\right)\left(-1 + \frac{R_{eq}}{R_2}\right) + \frac{1}{h_o}\right]\sqrt{h_o R_{eq}} \quad \text{(Eq 12)}$$

where plus and minus signs in A_1 and A_3 are designated to zones I and II, respectively. It is assumed that no axial forces are applied at the exit side of the roll gap, and so the boundary conditions on the entry and exit are

$$\sum F_x = (\sigma_1 - \sigma_2)\frac{dh}{2} = 0 \quad \text{at} \quad x = 0 \text{ and } x = L \quad \text{(Eq 13)}$$

Substituting Eq 6 and 11 into 10 and using the subsequent results with Eq 13, the constants C_1 for zones I and II are obtained as follows:

Zone I

$$C_{1,I} = k\left(1 + \sqrt{1 - m^2}\right)(1 - Ln(h_o)) \quad (0 \le x \le x_n)$$

Zone II

$$C_{1,II} = A_1 L + A_2\left[1 - \mathrm{Ln}\left(\frac{L^2}{R_{eq}} + h_o\right)\right] + A_3 \arctan\left(\frac{L}{\sqrt{h_o R_{eq}}}\right) - \frac{1}{2}mkL\left(\frac{1}{R_1} + \frac{1}{R_{eq}}\right) \quad (x_n \le x \le L) \quad \text{(Eq 14)}$$

where A_1 and A_3 (with plus sign), and A_2 are given by (12).

2.2 Ring Rolling Force

If the contact angle of the rolls and that of the ring is assumed to be small, then the rolling force is given by

$$F_1 = \int_0^{x_n}\left(P_{1,I} - mk\frac{x}{R_1}\right)dx + \int_{x_n}^{L}\left(P_{1,II} + mk\frac{x}{R_1}\right)dx \quad \text{(Eq 15)}$$

where $P_{1,I}$ and $P_{1,II}$ are the main roll pressures at the zone I and II, respectively, and x_n is the neutral point where the pressures at zones I and II become equal. Substituting Eq 11 into 15 and integrating the terms, the rolling force per unit width of the ring is obtained as follows:

$$F_1 = \left(A_1 - \frac{mk}{R_1}\right)\left(x_n^2 - \frac{L^2}{2}\right) + A_2\left[L\cdot\left(Ln\left(\frac{L^2}{R_{eq}} + h_o\right) - 2\right) + 2\sqrt{h_o R_{eq}}\arctan\left(\frac{L}{\sqrt{h_o R_{eq}}}\right)\right] + A_3\left[\frac{1}{2}\sqrt{h_o R_{eq}}.Ln\left(1 + \frac{L^2}{h_o R_{eq}}\right) - L\cdot\arctan\left(\frac{L}{\sqrt{h_o R_{eq}}}\right) + 2x_n\cdot\arctan\left(\frac{x_n}{\sqrt{h_o R_{eq}}}\right) - \sqrt{h_o R_{eq}}\cdot\mathrm{Ln}\left(1 + \frac{x_n^2}{h_o R_{eq}}\right)\right] + C_{1,I}x_n + C_{1,II}(L - x_n) \quad \text{(Eq 16)}$$

where A_1 and A_3 (with plus sign), and A_2 are given by (12) and $C_{1,I}$ and $C_{1,II}$ given by (14), respectively.

2.3 Ring rolling Torque

The rolling torque is an important parameter which determines the energy consumption of the ring rolling mill. As mandrel is idler, the total torque is exerted on the ring individually by the main roll. The ring rolling torque per unit width of the ring can be calculated by integrating the moment of the frictional shear force along the arc length of contact around the roll axis as follows:

$$T_1 = R_1\left(-\int_0^{x_n} mk\,dx + \int_{x_n}^{L} mk\,dx\right) = R_1 mk\left(-\int_0^{x_n} dx + \int_{x_n}^{L} dx\right) = R_1 mk(L - 2x_n) \quad \text{(Eq 17)}$$

3. Results and Discussion

From the mathematical model presented above, the effects of factors on the ring rolling process are investigated. The effect of friction factor on rolling pressure distributions for the main roll and the mandrel are considered in Fig. 5. It is seen that with increasing friction factor, the specific rolling pressure of the main roll and the mandrel decrease with a positive rate and the neutral point approaches the entry. Furthermore, a jump in mandrel pressure distribution at the neutral point is noticeable. An important physical reason for this is the direction of friction force at the main roll and ring interface which is suddenly changed at this point. Therefore, the magnitude of the mandrel pressure is consequently changed abruptly to hold the equilibrium condition in both the vertical and horizontal directions.

The normal stresses on the vertical side of element at the top and bottom of the slab for various friction factors are shown in Fig. 6. Unlike the results shown in Fig. 3, the normal stresses at the top and bottom of the slab have negative and positive signs, respectively. The magnitudes of normal stresses at both the top and bottom of the slab increase with increasing friction factor.

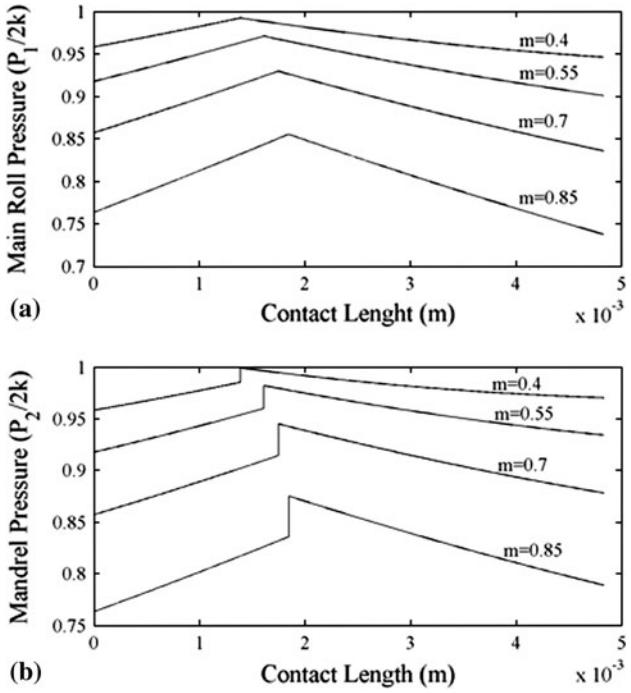

Fig. 5 The specific ring rolling pressure of (a) the main roll and (b) the mandrel for various friction factors ($R_1 = 100\,\text{mm}, R_2 = 50\,\text{mm}$, $R_3 = 70\,\text{mm}$, $n = 2\,\text{rev/s}$, $h_o = 10\,\text{mm}$, $v = 1\,\text{mm/s}$)

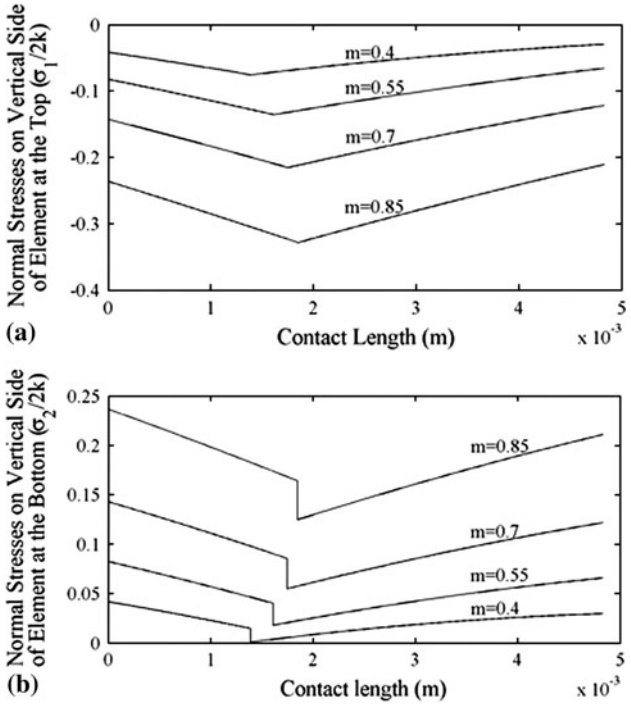

Fig. 6 Normal stresses on vertical side of element (a) at the top of the slab and (b) at the bottom of the slab for various friction factors ($R_1 = 100\,\text{mm}$, $R_2 = 50\,\text{mm}$, $R_3 = 70\,\text{mm}$, $n = 2\,\text{rev/s}$, $h_0 = 10\,\text{mm}$, $v = 1\,\text{mm/s}$)

Furthermore, from entry and exit to the neutral point, the magnitudes of normal stresses at the top increase and at the bottom decrease. An uneven residual stress distribution at the resulting rings is one of the main problems which have negative

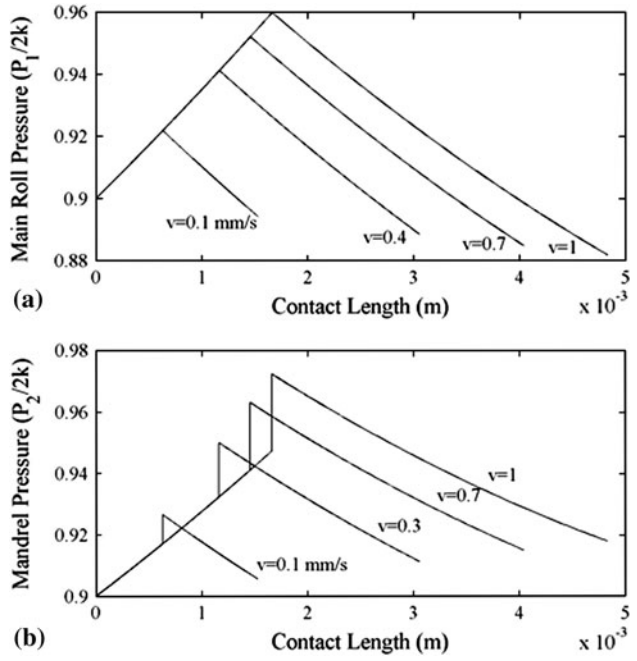

Fig. 7 The specific ring rolling pressure of (a) the main roll, (b) the mandrel for various feed speeds ($R_1 = 100\,\text{mm}$, $R_2 = 50\,\text{mm}$, $R_3 = 70\,\text{mm}$, $n = 2\text{rev/s}$, $h_o = 10\,\text{mm}$, $m = 0.6$)

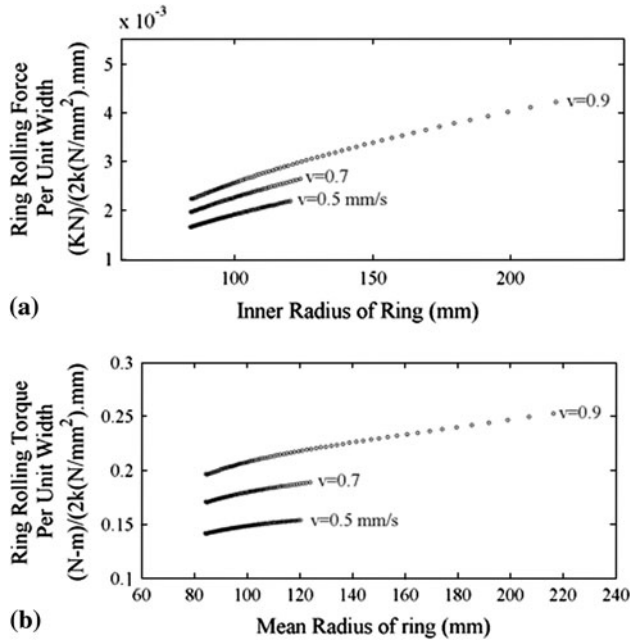

Fig. 8 The specific ring rolling (a) force and (b) torque for various feed speeds with respect to the current mean radius of ring ($R_1 = 275\,\text{mm}$, $R_2 = 45\,\text{mm}$, $R_3 = 60\,\text{mm}$, $R_m = 83.75\,\text{mm}$, $n = 0.78\,\text{rev/s}$, $m = 0.4$, $h_o = 47.5\,\text{mm}$)

economical implications. From this point of view, the lower the friction factor, the better the outcome. According to Eq 9, since the normal stress at the bottom of the slab depends directly on the mandrel pressure, there is also a jump in its distribution along the contact length.

Table 1 Analytic results of ring rolling process for different feed speeds

Feed speed, mm/s	Number of rotations	Contact length, mm	Neutral point, mm	Reduction in thickness, %	Mean ring radius, mm
0.5	90	4.5	1.7	35	120.2
0.7	80	6.1	2.3	49.5	123.8
0.9	70	7.8	3.0	61.3	216.25

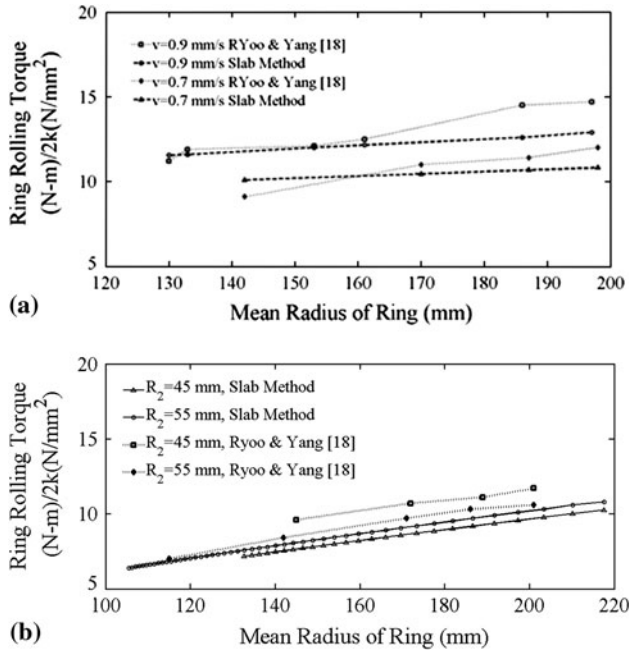

Fig. 9 Comparison of results for slab analysis and experimental studies. Effect of (a) feed speed and (b) radius of the mandrel on the ring rolling torque. ($R_1 = 275$ mm, $R_2 = 45$ mm, $R_3 = 60$ mm, $v = 0.7$ mm/s, $n = 0.78$ rev/s, $h_0 = 47.5$ mm, $m = 0.4, w = 52$ mm)

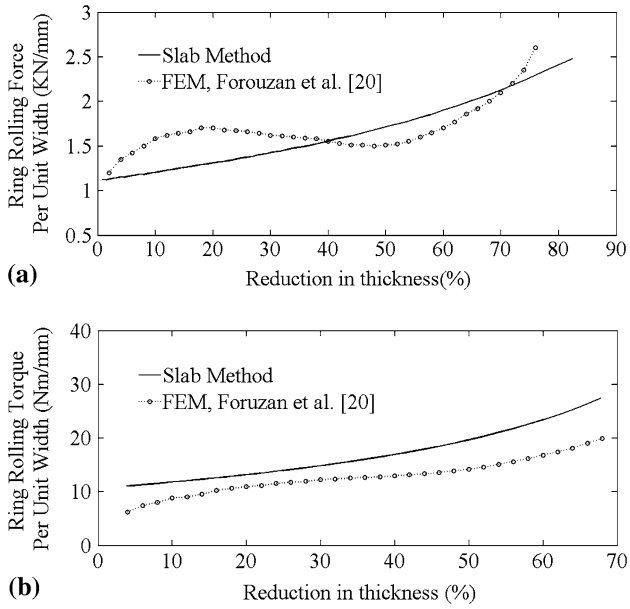

Fig. 10 Comparison of the specific ring rolling (a) force, (b) torque with respect to thickness reduction for modified slab analysis and FEM simulation ($R_1 = 114.3$ mm, $R_2 = 34.9$ mm, $R_3 = 38.1$ mm, $n = 0.52$ rev/s, $m = 0.3, v = 0.297$ mm/s, $h_o = 25.4$ mm) Material: aluminum - alloy HE 30 (0.8% Mg, 1% Si, 0.7% Mn)

In Fig. 7, the effect of the feed speed on the rolling pressure distributions for the main roll and the mandrel is observed. It is seen that the specific rolling pressure for the main roll and the mandrel increase with increasing feed speed, and the neutral point also approaches the entry side. In addition, a jump in mandrel pressure distribution at the neutral point is noticeable.

The force and torque with respect to the current mean radius of ring are shown in Fig. 8 for different values of feed speeds. Some other analytic results at the end of process are illustrated in Table 1. For any value of the feed speed, the force and torque increase slowly with increase in the ring mean radius. The slope of the curve at higher feed speed is larger than that at lower ones. It could also be seen that the force and torque increase with increasing feed speed, which indicates that a much higher force and torque are necessary to maintain the ring rolling process in the cases of relatively high pressing velocity and large ring mean radius.

In Fig. 9, the results of the slab method analysis and those of experimental studies by Ryoo and Yang (Ref 18) are compared. The effects of feed speed and radius of the mandrel on the ring rolling torque are evaluated in parts (a) and (b), respectively. It could be seen that the values for torque obtained from the slab method are in good agreement with experimental ones. For different feed speeds, the differences between two values increase with increasing ring mean radius, while the maximum deviations at 0.9 and 0.7 mm/s feed speeds are 12.5 and 9.8%, respectively. According to the other case, the slab method has more accurate results for the mandrel with the bigger radius. It means that the maximum differences between theoretical and experimental results for 45 and 55 mm mandrel radii are 19 and 6%, respectively.

Figure 10 shows results for ring rolling force and torque with respect to thickness reduction from the present modified slab method analysis and the FEM simulation (Ref 20). Again, it could be seen that the values for force and torque obtained from the present method are in good agreement with FEM results.

4. Conclusions

Using different feed speeds and friction factors, ring rolling process was investigated by applying the slab method. It was found that with increasing friction factor or decreasing feed speed, specific rolling pressure of main roll and mandrel decrease, and the neutral points approach the entry and exit, respectively, but uneven residual stresses increase. Further-

more, a jump in mandrel pressure distribution as a result of change in the direction of frictional force at the neutral point is noticeable. For any value of the feed speed, the force and torque required for ring rolling process increase slowly with the ring mean radius. The accuracy of this analysis was verified using reference (Ref 18) experimental data and the authors' FEM analysis (Ref 20).

References

1. S. Casotto, F. Pascon, A.M. Habraken, and S. Bruschi, Thermo-Mechanical-Metallurgical Model to Predict Geometrical Distortions of Rings During Cooling Phase After Ring Rolling Operations, *Int. J. Mach. Tools Manuf.*, 2005, **45**, p 657–664
2. J.M. Allwood, R. Kopp, D. Michels, O. Music, M. Oztop, T.F. Stanistreet, A.E. Tekkaya, and I. Tiedemman, The Technical and Commercial Potential of an Incremental Ring Rolling Process, *J. Manuf. Technol.*, 2005, **54**, p 233–236
3. W. Johnson and G. Needham, Experiments on Ring Rolling, *Int J. Mech. Sci*, 1968, **10**, p 95–113
4. V. Ranatunga and J.S. Gunasekera, UBET-Based Numerical Modeling of Bulk Deformation Processes, *J. Mater. Eng. Perform.*, 2007, **15**, p 47–52
5. J.B. Hawkyard, W. Johnson, J. Kirkland, and E. Appleton, Analysis of Roll Force and Torque in Ring Rolling, With Some Supporting Experiments, *Int. J. Mech. Sci.*, 1973, **15**, p 873–893
6. A.G. Mamalis, W. Johnson, and J.B. Howkyard, Pressure Distribution, Roll Force and Torque in Cold Ring Rolling, *J. Mech. Eng. Sci.*, 1976, **18**(4), p 196–209
7. D.Y. Yang, J.S. Ryoo, J.C. Choi, and W. Johnson, Analysis of Roll Torque in Profile Ring Rolling of L-ections, *Proc. of the 21th Int. MTDR Conf.*, 1980 (London), p 69–74
8. J.S. Ryoo, D.Y. Yang, and W. Johnson, Ring Rolling: The Inclusion of Pressure Roll Speed for Estimating Torque by using a Velocity Superposition Method, *Proc. of the 24th Int. MTDR Conf.*, 1983 (Manchester), p 19–24
9. K. Davey and M.J. Ward, A Practical Method for Finite Element Ring Rolling Simulation Using the ALE Flow Formulation, *Int. J. Mech. Sci.*, 2002, **44**, p 165–190
10. M.R. Forouzan, M. Salimi, and M.S. Gadala, Three-Dimensional FE Analysis of Ring Rolling by Employing Thermal Spokes Method, *Int. J. Mech. Sci.*, 2003, **45**, p 1975–1998
11. L. Dewasurendra, "A Finite Element Method for Ring Rolling Process," Ph.D Thesis, Ohio University, 1998
12. G.Y. Tzou, Relationship Between Frictional Coefficient and Friction Factor in Asymmetrical Sheet Rolling, *J. Mater. Process. Technol.*, 1999, **86**, p 271–277
13. M. Salimi and M. Kadkhodaei, Slab Analysis of Asymmetrical Sheet Rolling, *J. Mater. Process. Technol.*, 2004, **150**, p 215–222
14. H. Gaoa, S.C. Ramalingama, G.C. Barbera, and G. Chen, Analysis of Asymmetrical Cold Rolling With Varying Coefficients of Friction, *J. Mater. Process. Technol.*, 2002, **124**, p 178–182
15. Y.M. Hwang and G.Y. Tzou, Analytical and Experimental Study on Asymmetrical Sheet Rolling, *Int. J. Mech. Sci.*, 1997, **39**(4), p 289–303
16. M. Salimi and F. Sassani, Modified Slab Analysis of Asymmetrical Plate Rolling, *Int J. Mech. Sci*, 2002, **44**, p 1999–2023
17. Y.M. Hwang and G.Y. Tzou, An Analytical Approach to Asymmetrical Cold and Hot Rolling of Clad Sheet Using the Slab Method, *J. Mater. Process. Technol.*, 1995, **62**, p 249–259
18. J.S. Ryoo and D.Y. Yang, The Influence of Process Parameters on Torque and Load in Ring Rolling, *J. Mech. Work. Technol.*, 1986, **12**, p 307–321
19. H. Lin and Z.X. Zhi, The Extremum Parameters in Ring Rolling, *J. Mater. Process. Technol.*, 1997, **69**, p 273–276
20. M.R. Forouzan, M. Salimi, M.S. Gadala, and A.A. Aljawi, Guide Roll Simulation in FE Analysis of Ring Rolling, *J. Mater. Process. Technol.*, 2003, **142**, p 213–223